Journal of the Optical Society of Korea, Vol. 7, No. 2, June 2003, pp. 119-125

Observation of Parametric Resonance in a Magneto-Optical Trap

Heung-Ryoul Noh

Department of Physics, Chonnam National University, Gwangju 500-757, KOREA

Kihwan Kim, Hyun-Ji Ha, and Wonho Jhe*

School of Physics and Center for Near-field Atom-photon Technology, Seoul National University, Seoul 151-742, KOREA

(Received March 3, 2003)

We demonstrate parametric resonance in a magneto-optical trap. When we modulate the intensity of the cooling laser at about twice the resonant frequency of the trap, the atoms in the trap are divided into two parts and oscillate with 180 degree phase difference with the finite length due to nonlinearity of the trap potential. These are the effects of general nonlinear dynamics, called the Hopf bifurcation, or limit cycle motion. The amplitude and the phase of the oscillations are measured and compared with the theoretical calculations based on simple Doppler cooling theory. The experimental results are in excellent agreement with the simulation results based on the simple Doppler cooling theory.

OCIS codes : 020.7010, 300.6210.

I. INTRODUCTION

A magneto-optical trap (MOT) [1] has been widely used in a large number of experiments of atomic and optical physics, such as atomic beam, cold collision, nonlinear optics, and atom optics. Many researches about the dynamics of the MOT have been carried out experimentally and theoretically, including the understanding the lower temperature than Doppler limit [2,3], the phase space density [4], and the lifetime of the trap, etc. The nonlinear dynamics of MOT, however, has seldom been studied, except for considering the shadow effect due to the optical thickness of the atomic cloud [5] and in the case where the trapping beams are misaligned [6], even though the equation of MOT has some nonlinearities. To our knowledge, no systematic studies of these nonlinearities have been performed through the modulation of cooling laser intensities or magnetic field gradients, that is the trap potentials. The modulation of the potential depth was often used to measure the vibrational frequencies in an optical lattice or a simple dipole trap. [7] In such measurements only fluorescence of the atoms in the traps after the modulation have been observed. However, the dynamics of atoms escaping the traps during the modulation have not been investigated.

The experiments on the modulation of the cooling lasers are very similar to those of parametric pumped electron oscillators in the Penning trap. [8–10] The simple observed features of an electron in the cylindrical Penning trap are related to cooperative behavior and nonlinear dynamics. The electron oscillators exhibit a rich and varied nonlinear dynamics which our systems also manifested. The striking feature of our system is that it can visualize the collective motion and nonlinear dynamics, which have been detected indirectly by measuring the induced currents in the Penning trap.

In this paper, we present the theoretical and experimental results of the parametrically driven MOT by using the modulation of the MOT potential, especially the cooling laser intensity. When we modulate the intensity of the cooling laser at about twice the resonant frequency of the trap, the atoms in the MOT are divided into two parts and oscillate reciprocally with the finite length due to nonlinearity of the trap. The amplitude of oscillation and the phase with respect to the modulation of the cooling laser are measured with the images of the atomic cloud and compared to the theoretical calculations.

II. PARAMETRIC RESONANCE AND LIMIT CYCLE

1. Equation of Motion

We describe the atomic motion in the parametrically driven MOT in terms of simple Doppler cooling theory. The magnetic field in the MOT is given by

$$\vec{B} = b(-\frac{x}{2}\hat{x} - \frac{y}{2}\hat{y} + z\hat{z}), \tag{1}$$

where b is the magnetic field gradient for the z-axis. The $\sigma^+(\sigma^-)$ polarized light propagates from the $-z(+z)$ axis, while the $\sigma^-(\sigma^+)$ polarized light propagates from the $-x(+x)$ and $-y(+y)$ axis. The laser intensities are modulated to excite the parametric resonance. In this study we only excite the parametric resonance for the z-axis. If we vary the parameters such as laser intensity and detuning, we can excite the resonance for other axes. Note that it is also interesting to study the coupling effect between different axes. When we consider atomic motion only for the z-axis, the saturation parameter is given by $s_0(1+\varepsilon\cos\omega t)$, where ε is the modulation amplitude, ω is the modulation frequency, and $s_0 = I/I_s$ is the unmodulated saturation parameters with I being the laser intensity of a laser beam for z-axis and I_s (=1.62 mW/cm^2) being the saturation intensity for a ^{85}Rb atom.

Including the random recoil from the spontaneously emitted photons, the atomic motion can be described by the following equation for a two-level atom [3],

$$m\ddot{z} = f(z,\dot{z},t) + f_r(t)\,, \tag{2}$$

where $f(z,\dot{z},t)$ is the radiation pressure force from the counterpropagating laser beams and f_r is the random force from the spontaneous emissions. When we consider only the Doppler cooling force $f(z,\dot{z},t)$ is given by

$$f(z,\dot{z},t) = \frac{\hbar k\Gamma}{2}\left[\frac{s_0(1+\varepsilon\cos\omega t)}{1+s_0(1+\varepsilon\cos\omega t)+4(\delta - k\dot{z} - \frac{\mu_B b}{\hbar}z)^2/\Gamma^2} - \frac{s_0(1+\varepsilon\cos\omega t)}{1+s_0(1+\varepsilon\cos\omega t)+4(\delta + k\dot{z} + \frac{\mu_B b}{\hbar}z)^2/\Gamma^2}\right], \tag{3}$$

where k is the wave vector, μ_B is Bohr magneton, m is the mass of an atom, Γ is the decay rate of the excited state (=$2\pi\times$5.9 MHz), and $\delta = (\omega_L - \omega_A)$ is the detuning of the laser frequency ω_L relative to the atomic resonance frequency ω_A. Since the random force only contributes to the widths of the spatial or velocity distribution, it will be ignored for the time being as far as the center of mass motions are concerned. The discussions on the random force will be presented at the end of this section.

If we consider the terms in third orders in position (z) and velocity ($\dot{z}$), Eq. (2) can be approximately written by

$$\ddot{z} + \beta\dot{z} + \omega_0^2(1+\varepsilon\cos\omega t)z = -A_0\omega_0^2\left[z + \frac{\beta}{\omega_0^2}\dot{z}\right]^3, \tag{4}$$

where

$$\beta = \frac{8\hbar k^2 s_0(-\delta/\Gamma)}{m\left[1+4(\delta/\Gamma)^2\right]^2}, \tag{5}$$

$$\omega_0 = \sqrt{\frac{\mu_B b}{\hbar k}\beta}, \tag{6}$$

$$A_0 = 8\left(\frac{\mu_B b}{\hbar\Gamma}\right)^2\frac{4(\delta/\Gamma)^2 - 1}{\left[(\delta/\Gamma)^2+1\right]^2}. \tag{7}$$

Here we have assumed that $\varepsilon \ll 1$ and the damping is weak, that is, $\beta \ll \omega_0$.

If we neglect the nonlinear terms in Eq. (4), it becomes a typical Mathieu equation [11,12]. The solutions of a Mathieu equation show the parametric resonance which occurs when the modulation frequency $\omega = 2\omega_0$, where ω_0 is the natural frequency (Eq. (6)). As shown in Fig. 1(a), the parametric resonance occurs in the range $2\omega_0 - \varepsilon\omega_0/2 < \omega < 2\omega_0 + \varepsilon\omega_0/2$ (dotted lines). Here the horizontal axis is the modulation amplitude (ε), and the vertical axis is the modulation frequency normalized to the trap frequency (ω/ω_0). When the modulation frequency lies inside this region, the solution diverges. If we take into account the damping, the parametric resonance range becomes $\omega_1 < \omega < \omega_2$ (dotted curve in Fig. 1), where ω_1 and ω_2 are given by

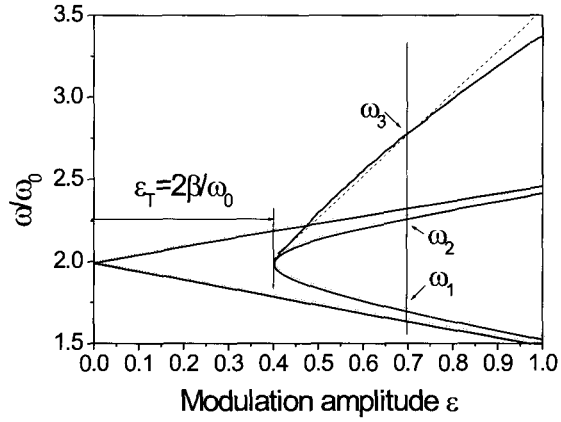

FIG. 1. For given b, δ and s_0, the instability region of parametrically driven MOT is plotted. The horizontal axis is the modulation amplitude, and the vertical axis is the frequency of modulation relative to the natural trap frequency. When the experimental parameters reside inside the interested region, the solutions diverge or show the limit cycle motions.

$$\omega_1 = 2\omega_0 - \frac{\omega_0}{2}\sqrt{\varepsilon^2 - \varepsilon_T^2}\,,$$
$$\omega_2 = 2\omega_0 + \frac{\omega_0}{2}\sqrt{\varepsilon^2 - \varepsilon_T^2}\,. \quad (8)$$

Here $\varepsilon_T = 2\beta/\omega_0$ is the threshold value above which the parametric resonance can occur.

Now let us include the nonlinear terms (Eq. (4)). Note that the detailed results are presented in Fig. 1 as solid lines and curves, which will be described in the next subsection. In the steady-state regime in the rotating frame with the angular frequency $\omega/2$, the solutions of Eq. (4) can be written by

$$z(t) = R(t)\cos\left[\frac{\omega}{2}t + \psi(t)\right]\,, \quad (9)$$

where the amplitude $R(t)$ and the phase $\psi(t)$ satisfy the following equations:

$$\frac{dR}{dt} = -\frac{\beta}{2}R\left[1 + \frac{3}{16}(4+\varepsilon_T^2)A_0R^2 - \frac{\varepsilon}{\varepsilon_T}\sin 2\psi\right] \quad (10)$$
$$\frac{d\psi}{dt} = -\frac{\omega - 2\omega_0}{2} + \frac{\varepsilon\omega_0}{4}\cos 2\psi + \frac{3}{32}(4+\varepsilon_T^2)A_0\omega_0R^2$$

Here we have used an averaging method. [12]

The atomic motion can be described more clearly in the rotating frame with the angular velocity of $\omega/2$. In that frame, Eq. (10) can be transformed to the following equations:

$$\frac{dq_1}{dt} = -\frac{\beta}{2}q_1\left(1 + B_0R^2\right) + \frac{\omega_0}{2}B_0\left(\zeta + \Omega - R^2\right)q_2\,,$$
$$\frac{dq_2}{dt} = -\frac{\beta}{2}q_2\left(1 + B_0R^2\right) + \frac{\omega_0}{2}B_0\left(\zeta - \Omega + R^2\right)q_1\,, \quad (11)$$

where we have used $q_1 = R\cos\psi$ and $q_2 = R\sin\psi$.

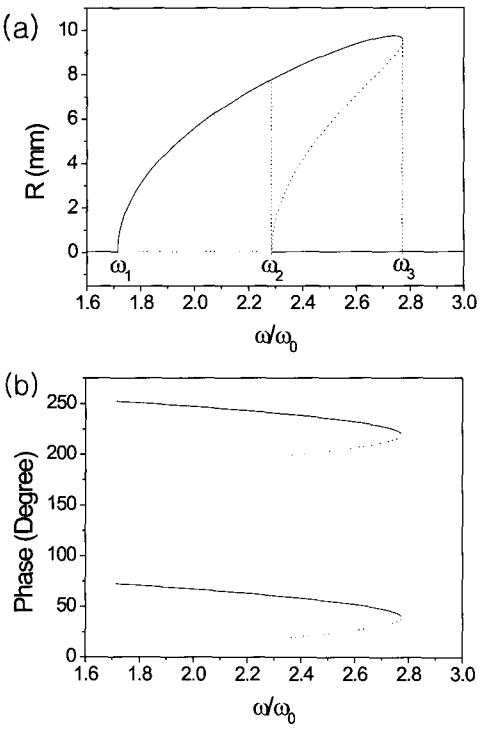

FIG. 2. The calculated solutions of amplitude R (a) and phase ψ (b) of the atomic motion ($\varepsilon = 0.7$). The solid (dotted) curves denote stable (unstable) solutions. In Fig. 2(a) we can observe hysteresis.

Here

$$B_0 = \frac{3(4+\varepsilon_T^2)}{16}A_0, \quad \zeta = \frac{\varepsilon}{2B_0}, \text{ and } \quad \Omega = \frac{\omega - 2\omega_0}{\omega_0 B_0}\,.$$

2. Discussion of the Solutions

As well as a trivial solution $R = 0$, we have the nontrivial steady-state solutions for Eq. (10) as

$$R^2 = \frac{16}{3A_0(4+\varepsilon_T^2)^2} \times \left\{4(\eta - 2) - \varepsilon_T^2 \pm \sqrt{\varepsilon^2(4+\varepsilon_T^2) - 4\varepsilon_T^2(\eta-1)^2}\right\}\,,$$
$$\cos 2\psi = \frac{2}{\varepsilon(4+\varepsilon_T^2)^2} \times \left\{\varepsilon_T^2(\eta - 1) \mp \sqrt{\varepsilon^2(4+\varepsilon_T^2) - 4\varepsilon_T^2(\eta-1)^2}\right\}\,, \quad (12)$$

where the upper (lower) sign denotes the stable (unstable) solutions. The calculated results for the amplitude and phase are shown in Fig. 2(a) and 2(b), respectively, where $\varepsilon = 0.7$. As can be seen in Fig. 2, there exist three frequencies (ω_1, ω_2 and ω_3) which characterize the existence of solutions. The frequencies ω_1 and ω_2 are defined in Eq. (8) and ω_3 is given by

$$\omega_3 = \omega_0\left(1 + \frac{\varepsilon}{2\varepsilon_T}\sqrt{4+\varepsilon_T^2}\right)\,. \quad (13)$$

Let us discuss the solutions. When $\omega_1 < \omega < \omega_2$, as

well as an unstable solution ($R = 0$), there exist two stable solutions, because we have two solutions of the phase with the difference of π. Ignoring the nonlinear terms, the solutions in this region become divergent. Due to the nonlinear terms, the solutions cease to diverge and have a finite value, which is called a limit cycle. The values ω_1 and ω_2 have the same values as in the linear case. This is because, in both cases, we only take into consideration up to the first order in ε. We have solved Eq. (2) to obtain the correct values of ω_1, ω_2 and ω_3 as shown in Fig. (1). The results are shown in Fig. 1 (solid curve for ω_1, ω_2; solid line for ω_3). We can see that ω_1 and ω_2 are slightly shifted towards smaller values. We can obtain analytical forms of the frequencies up to the second orders in ε and they are given by [12]

$$\omega_1 = \omega_0 \left(2 - \frac{1}{2}\sqrt{\varepsilon^2 - \varepsilon_T^2} - \frac{1}{32}\left(\varepsilon^2 + \varepsilon_T^2\right)\right),$$
$$\omega_2 = \omega_0 \left(2 + \frac{1}{2}\sqrt{\varepsilon^2 - \varepsilon_T^2} - \frac{1}{32}\left(\varepsilon^2 + \varepsilon_T^2\right)\right). \quad (14)$$

These results are almost equal to the results from the numerical calculations.

When $\omega_2 < \omega < \omega_3$, we have two unstable solutions as depicted in Fig . 2 (dotted line) and three stable solutions. Of three stable solutions, one is a stable attractor at the origin and the others are limit cycles with opposite phases. The frequency ω_3 is approximately linearly proportional to ε. The analytic form (Eq. (13)) and the result of numerical calculation are shown in Fig . 1. In our experimental condition, because ε is comparable to 1, the results for large amplitude are not so accurate. In the other frequency region ($\omega < \omega_1$ or $\omega > \omega_3$), we have one stable attractor at the origin.

When we increase the modulation frequency, the stable attractor at the origin converts to the limit cycle motion at the frequency $\omega = \omega_1$, which is called a super-critical Hopf bifurcation. [13] On the other hand, decreasing the frequency, we have sub-critical Hopf bifurcation at the frequency $\omega = \omega_2$, which is the conversion of stable attractor and limit cycles into the limit cycle motions. The experimental observation of super- and sub-critical bifurcation will be presented in the next section. Loosely we call the frequency region $\omega_1 < \omega < \omega_2$ the super-critical Hopf bifurcation region, while $\omega_2 < \omega < \omega_3$ is called the sub-critical Hopf bifurcation region.

The stability regions in the rotating frame are plotted in Fig. 3(a) for $\omega/\omega_0 = 2.5$ (sub-critical Hopf bifurcation region) and Fig. 3(b) for $\omega/\omega_0 = 2.0$ (super-critical Hopf bifurcation region). In Fig. 3 the stable (unstable) points are denoted by the filled circles (triangles). In Fig. 3(a) there exist three stable points

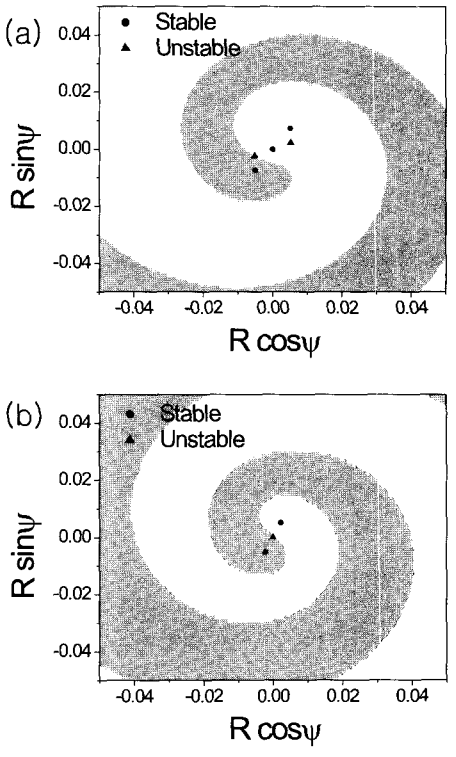

FIG. 3. The stability regions in the rotating frame at the frequency $\omega/\omega_0 = 2.5$ (a) and $\omega/\omega_0 = 2.0$ (b). Filled circles (triangles) represent stable (unstable) solutions.

and two unstable points. The regions are divided by three spiral-shaped regions. The atoms with initial conditions in one region converges to the stable point which belongs to that region. The unstable points lies at the border of the regions. In Fig. 3(b), there are two stability regions. We have two (one) stable (unstable) points. When the modulation frequency corresponds to the sub-critical Hopf bifurcation region, in the experiment, the initial conditions of trapped atoms reside in the central spiral-shaped region in Fig. 3(a). Thus we only observe the trap when the frequency is swept down across ω_3. On the other hand, when we sweep up the frequency crossing ω_2, we only observe the two limit cycle motions, because the initial conditions reside in the two large spirals. That is to say, we may observe hysteresis. However, in the sub-critical Hopf bifurcation region, as will be seen in the next section, we can always observe the limit cycle motions as well as the central trap independent of the direction of the frequency sweeping. This is because, in the experiment there always exists diffusion which provokes atoms to make transition from the fixed point to the limit cycle motions (Eq. (2)).

In order to understand the transitions between the fixed point and limit cycle motions or between two limit cycle motions, we need to solve Eq. (2) including the momentum diffusion. The subject of the transi-

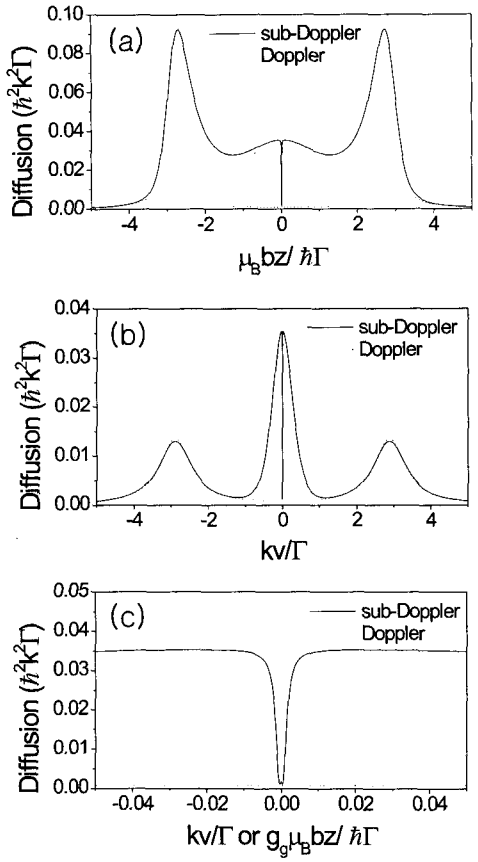

FIG. 4. The calculated momentum diffusion coefficients, (a) for $D_{zz}(z,0)$, (b) for $D_{zz}(0,v)$ and (c) for detailed plots at the center. The calculation is performed for the $5S_{1/2}, F = 3 \rightarrow 5P_{3/2}, F = 4$ cooling transition of ^{85}Rb atoms. The dotted curves denote the simple diffusion coefficients given by Eq. (16).

tions is currently under progress and will be reported elsewhere. In addition to the transitions, momentum diffusion contributes to the width of atoms in position or in velocity. In Eq. (2) the random force satisfies following equation:

$$< f_r(t) f_r(t') >= 2D_{zz}\delta(t-t') \,, \qquad (15)$$

where D_{zz} is the momentum diffusion tensor for z-axis and $< \cdots >$ denotes the time average. In Doppler cooling theory, the momentum diffusion coefficient is simply given by

$$D_{zz}(z,\dot{z}) = \frac{\hbar^2 k^2 \Gamma}{3}\left[\frac{s_0}{1+s_0+4(\delta - k\dot{z} - \frac{\mu_B b}{\hbar}z)^2/\Gamma^2} + \frac{s_0}{1+s_0+4(\delta + k\dot{z} + \frac{\mu_B b}{\hbar}z)^2/\Gamma^2}\right]. \qquad (16)$$

In the experiment, however, the spatial width is about 5 times larger than the simulation result with the momentum diffusion coefficient (Eq. (2)). It is somewhat difficult to explain the spatial width accurately. However we can obtain approximately reasonable results using the diffusion coefficient calculated by means of the sub-Doppler laser cooling theory [14]. The calculated momentum diffusion coefficients for the $5S_{1/2}, F = 3 \rightarrow 5P_{3/2}, F = 4$ cooling transition line of ^{85}Rb are presented in Fig. 4. $D_{zz}(z,0)$ and $D_{zz}(0,\dot{z})$ are shown in Fig. 4(a) and 4(b), respectively, where the solid lines denotes the results for the sub-Doppler theory and the dotted lines are the results of Eq. (16). Fig. 4(c) shows the result for the detailed plot of the central region. Here $g_g(= 1/3)$ denotes the Lande g-factor of the $5S_{1/2}, F = 3$ ground state. Note that, except the near region satisfying $k\dot{z}/\Gamma + g_g\mu_B bz/\hbar\Gamma = 0$, the diffusion coefficient is much larger than that for the simple Doppler theory. We have performed Monte-Carlo simulation using the equation of motion in Eq. (2), where the calculated momentum diffusion in Fig. 4 is adopted except for the sharp decrease near the central region. The results will be discussed in the next section.

III. EXPERIMENT

We study parametric resonance and limit cycle motion of atoms in a standard vapor-cell MOT where the intensity of cooling laser is modulated. We used the first order diffracted laser by an acousto-optic modulator (AOM), which can alter the laser power according to the applied voltage. The ^{85}Rb atoms in the MOT have three dimensional confinements with the natural frequency ω_0 ($\omega_0/\sqrt{2}$) for z (x or y)-axis, where ω_0 is defined in Eq. (6). In the experiment we can adjust and choose the magnetic field gradient, laser intensity, and detuning to excite the parametric resonance. In order to observe the parametric resonance and limit cycle motion in the MOT, the s_0 should be very small (< 0.1). In the experiment we excite parametric resonance for the z-axis (the axis of anti-Helmholtz coils).

Our experimental parameters are as follows. For the z-axis, the normalized laser intensity s_0, the magnetic field gradient b, the normalized laser detuning δ, and the modulation amplitude ε are 0.042, 9 G/cm, -2.9 Γ, and 0.9, respectively. On these conditions, the natural frequency of confinement along the z-axis is $\omega_0 = 2\pi \times 31.5$ Hz. In this case the threshold modulation amplitude is given by $\varepsilon_T = 0.4$. That is to say, the modulation amplitude should be larger than 0.4 to excite parametric resonance, even if the modulation frequency is exactly twice the resonance frequency. On the other hand, the normalized laser intensity for the x- or y-axis is about $2.5s_0$. Accordingly the corresponding threshold modulation amplitude is 0.9, which is not smaller than the modulation amplitude in the experiment. This is why only in the z-axis

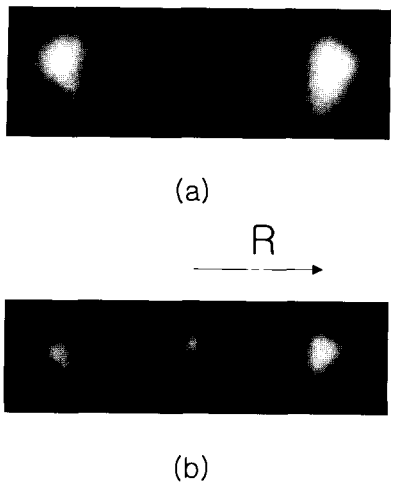

FIG. 5. The typical motions of atoms are shown at the modulation frequency of 75 Hz ($\omega/\omega_0 = 2.38$) for (a) and 95 Hz ($\omega/\omega_0 = 2.74$) for (b). Here the modulation amplitude is 0.9. Fig. 5 (a) shows super-critical bifurcation and Fig. 2 (b) shows sub-critical bifurcation.

there occurs parametric resonance, although the cooling laser intensities for all three directions are modulated at the same frequency and modulation amplitude. Note that, in some case, although the parametric resonance occurs for two or three directions, only the resonance for only one specific direction can be excited due to the coupling between different axes, which will be the subject of our next study.

When we modulate the intensity of the cooling laser at about twice its resonant frequency, the atoms in the MOT are divided and oscillate reciprocally with the finite length. The typical motions of atoms are shown in Fig. 5. The images of the cloud are taken every 1 ms for 1/2400 s of exposure time. Here, the modulation frequencies are 75 Hz ($\omega/\omega_0 = 2.38$) for (a) and 95 Hz ($\omega/\omega_0 = 2.74$) for (b), and the modulation amplitude is 0.9. Fig. 5(a) shows super-critical Hopf bifurcation and Fig. 5(b) shows sub-critical Hopf bifurcation. As explained in Fig. 2 or 3, we have two stable points (limit cycles) in super-critical region (Fig. 5(a)) and three stable points (one fixed point and two limit cycles) in sub-critical region (Fig. 5(b)). Due to the diffusion, as mentioned in the preceding section, three stable points (one is trap and two are limit cycle motions) can be observed always in Fig. 5(b). In Fig. 5(b) we can observe a bright small trap as well as the broad cloud. It can be attributed to the trapped atoms in the double potential of the MOT, which originates from the coherence of ground states via two-photon transitions. [14] The detailed study of the double structure of the MOT potential will be reported in a separate publication.

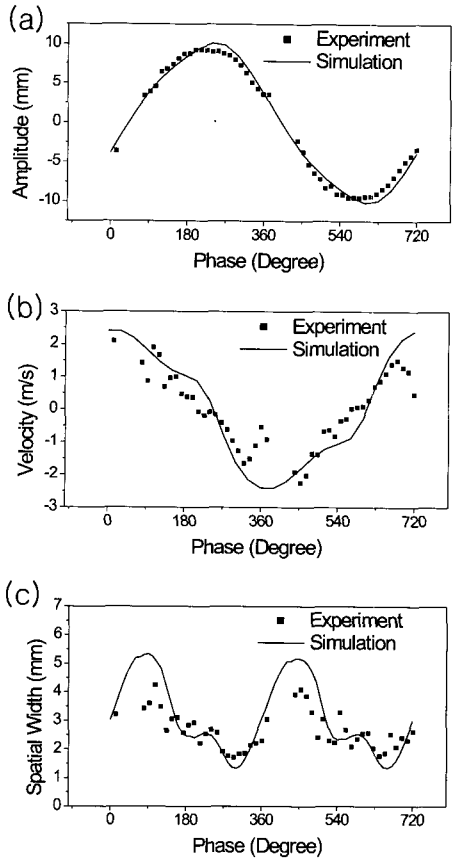

FIG. 6. The measured (points) and calculated results for the positions (a), velocities (b), and the spatial widths of the atoms as functions of the phase. Here the phase 720 degree corresponds to the elapsed time of $4\pi/\omega$ with ω the modulation frequency.

From the captured images we can measure the positions, velocities, and width of positions of the atomic cloud at each phase of modulation. Fig. 6 shows how (a) the positions, (b) the velocities and (c) the spatial width of the two atomic clouds depend on the phase. Here the phase 720 corresponds to the elapsed time of $4\pi/\omega$ with ω the modulation frequency. We follow one of two oscillating clouds with the phase difference of π. We can obtain Fig. 6(b) by differentiating the result of Fig. 6(a). From Fig. 6 we deduce the length of limit cycle and the phase delay with respect to the modulation of the cooling laser. Here, the points are obtained from experiments and the solid lines are from calculations. In Fig. 6(b) the shape of the velocity variation as the phase varies is not harmonic but looks like a relaxation oscillation, which is typical of nonlinear oscillations. Fig. 6(c) shows the width of the atomic cloud at different phases. The points are the experimental results and the line is the simulation result. The Monte-Carlo simulation has been carried out taking

into account the spontaneous emission as described in the preceding section. We can see the agreement between the experiment and simulation. In our experimental conditions, we were not able to measure the width of the velocity of the atomic clouds.

IV. CONCLUSION

In a Penning trap experiment, the problem of fluctuation-induced switching between the two stable states of a bistable system has been studied [10]. Contrary to the Penning trap experiment, in our system, the two dynamical states are visualized so that the switchings or the transitions between two dynamical states, far from the equilibrium, could be investigated better. Moreover, because the number of particles in the trap is much larger, we can also study the many body effects in the transitions.

In conclusion, we have studied the nonlinearity of MOT in terms of limit cycle. We have observed the parametric resonances, limit cycle motions, and Hopf bifurcation. We also have compared the experimental results with simulations in the amplitude of limit cycle motion, the phase with respect to the modulation drive, and the widths of atom clouds, and found that both are in good agreement. The two atomic clouds which were produced by parametric resonances could be a very special atomic beam, of which velocity and width of velocities are well controlled. Moreover, with this system many other interesting features of physics, such as the transitions between far equilibrium dynamical states can be studied.

ACKNOWLEDGEMENTS

This work was supported by the Creative Research Initiative Project of the Korea Ministry of Science and Technology.

*Corresponding author : whjhe@snu.ac.kr.

REFERENCES

[1] E. Raab, M. Prentiss, A. Cable, S. Chu, and D. Pritchard, "Trapping of Neutral Sodium Atoms with Radiation Pressure," *Phys. Rev. Lett.*, vol. 59, no. 23, pp. 2631-2634, 1987.

[2] J. Dalibard and C. C.-Tannoudji, "Laser Cooling Below the Doppler Limit by Polarization Gradients - Simple Theoretical Models," *J. Opt. Soc. Am. B*, vol. 6, no. 11, pp. 2023-2045, 1989.

[3] P. D. Lett, W. D. Phillips, S. L. Rolston, C. E. Tanner, R. N. Watts, and C. I. Westbrook, "Optical Molasses," *J. Opt. Soc. Am. B*, vol. 6, no. 11, pp. 2084-2107, 1989.

[4] C. G. Townsend, N. H. Edwards, C. J. Cooper, K. P. Zetie, C. J. Foot, A. M. Steane, P. Szriftgiser, H. Perrin, and J. Dalibard, "Phase-Space Density in the Magnetooptical Trap," *Phys. Rev. A*, vol. 52, no. 2, pp. 1423-1440, 1995.

[5] D. Wilkowski, J. Ringot, D. Hennequin, and J. C. Garreau, "Instabilities in a Magneto-Optical Trap: Noise-Induced Dynamics in an Atomic System," *Phys. Rev. Lett.*, vol. 85, no. 9, pp. 1839-1842, 2000.

[6] T. Walker, D. Sesko, and C. Wieman, "Collective Behavior of Optically Trapped Neutral Atoms," *Phys. Rev. Lett.*, vol. 64, no. 4, pp. 408-411, 1990.

[7] S. Friebel, C. D'Andrea, J. Walz, M. Weitz, and T. W. Hänsch, "CO_2-laser optical lattice with cold rubidium atoms," *Phys. Rev. A*, vol. 57, no. 1, pp. R20-R23, 1998.

[8] J. Tan and G. Gabrielse, "Synchronization of Parametrically Pumped Electron Oscillators with Phase Bistability," Phys. Rev. Lett., vol. 67, no. 22, pp. 3090-3093, 1991; J. Tan and G. Gabrielse, "Parametrically Pumped Electron Oscillators," *Phys. Rev. A*, vol. 48, no. 4, pp. 3105-3121, 1993.

[9] C. H. Tseng, D. Enzer, G. Gabrielse, and F. L. Walls, "1-bit memory using one electron: Parametric oscillations in a Penning trap," *Phys. Rev. A*, vol. 59, no. 3, pp. 2094-2104, 1999.

[10] L. J. Lapidus, D. Enzer, and G. Gabrielse, "Stochastic Phase Switching of a Parametrically Driven Electron in a Penning Trap," *Phys. Rev. Lett.*, vol. 83, no. 5, pp. 899-902, 1999.

[11] L. D. Landau and E. M. Lifshitz, *Mechanics* (Pergamon, London, UK, 1976).

[12] N. H. Nayfeh and D. T. Moore, *Nonlinear Oscillations* (Wiley, New York, USA, 1979).

[13] S. H. Strogatz, *Nonlinear Dynamics and Chaos* (Perseus, New York, USA, 2001).

[14] S. Chang and V. Minogin, "Density-matrix approach to dynamics of multilevel atoms in laser fields," *Phys. Rep.*, vol. 365, pp. 65-143, 2002.